Optical Engineering

SPIEDigitalLibrary.org/oe

Method of analysis for determining and correcting mirror deformation due to gravity

James H. Clark, III
F. Ernesto Penado

Optical Engineering 53(1), 015102 (January 2014)

Method of analysis for determining and correcting mirror deformation due to gravity

James H. Clark, III[a,*] **and F. Ernesto Penado**[b]
[a]Naval Research Laboratory/NPOI, 10391 W. Observatory Road, Flagstaff, Arizona 86001
[b]Northern Arizona University, Department of Mechanical Engineering, Flagstaff, Arizona 86011

Abstract. The Navy Precision Optical Interferometer, located near Flagstaff, Arizona, is a ground-based interferometer that collects, transports, and modulates stellar radiation from up to six primary flat collectors, known as siderostats, through a common vacuum relay system to a combiner. In the combiner, the modulated beams are superimposed, fringes obtained, and data recorded for further analysis to produce precise star positions or stellar details. The current number of observable stellar objects for the astrometric interferometer can increase from 6000 to at least 47,000 with the addition of full-aperture 20-deg down-tilting beam compressors in each optical train. Such an aperture increase, from the current 12.5 to 35 cm, opens the sky to many additional and fainter stars. Engineering analysis of our beam compressor primary mirror shows that the maximum allowable sag, 21 nm, occurs prematurely at 2.8-deg down-tilt angle. Furthermore, at the operational down-tilt angle of 20 deg, the wavefront deformation increases to 155 nm. We present a finite element analysis technique and design modification concept to reduce tilt-induced deformation on the mirror surface. This work is a first pass to determine the feasibility for a mechanical solution path forward. From this analysis, we found that four outwardly applied 17.8-N forces on the rear surface of the mirror could reduce sag from 155 to 32 nm at 20-deg down-tilt angle. [DOI: 10.1117/1.OE.53.1.015102]

Keywords: optical interferometry; beam compressor; off-axis optics; Navy Precision Optical Interferometer; tilted mirror deformations; finite element analysis; gravity-induced sag; nonsymmetric mirrors.

Paper 131334P received Aug. 29, 2013; revised manuscript received Nov. 17, 2013; accepted for publication Dec. 4, 2013; published online Jan. 9, 2014.

1 Introduction

1.1 *Overview*

The Navy Precision Optical Interferometer (NPOI), near Flagstaff, Arizona, makes use of smaller separate optical stations spaced along a Y-array and used simultaneously to simulate an equivalent single larger telescope (see Fig. 1). This ground-based instrument is useful in generating and upgrading existing astronomical catalogs and investigating synthetic aperture optical imaging techniques.[1] The NPOI is a joint effort between the Naval Research Laboratory and the US Naval Observatory in collaboration with the Lowell Observatory. There are currently two separate instruments combined at the NPOI: a 4-element stationary astrometric array and a 6-element reconfigurable imaging array. Both use flat-mirror tracking siderostats as primary light collectors that redirect stellar radiation through an evacuated beam relay system to a beam combiner station, where the beams are superposed, fringes obtained and modulated, and data recorded for further analysis. The original instrument design specifies star-tracking siderostats with flat mirrors that convey stellar radiation directly into static off-axis beam compressors. The inclusion of beam compressors allows fainter stars to be studied and cataloged, effectively increasing the number of observable stellar objects from the current 6,000 without beam compressors to approximately 47,000.

At each optical station, tracked stellar light is reflected through local atmosphere from a 35-cm clear aperture flat mirror, known as a siderostat, toward a 12.5-cm clear aperture active flat tip–tilt mirror.[2] The clear aperture is 3 cm less than the physical diameter of the mirror due to the mount. The tip/tilt mirror is located at the entry point of the evacuated beam relay system along a line projected 20 deg above the horizontal from the pivot of the siderostat. It is within this region that the off-axis beam compressor will reside. The stellar beam propagates from the tip/tilt mirror downward, then through a series of relay transport mirrors and ultimately to the beam combiner, where fringes are generated for further study. Path lengths from siderostat station to beam combiner range between 100 and 775 m, depending on the specific configuration of the array. We currently transport two to six separate beams to the combiner depending on the stellar observation program. Figure 2 shows a schematic of the passive relay transport light path plus the location of the intended off-axis beam compressor.

The off-axis beam compressor is a static nontracking optomechanical device. Tracking is performed by the siderostat and fast tip–tilt mirror combination. The reflected clear aperture of the siderostat is 35 cm; the fast tip–tilt mirror and transport optics only have a clear aperture of 12.5 cm. In the absence of the beam compressor, tracking and transport of the stellar beam remain the same, the difference being anything outside the 12.5-cm portion of the stellar light is discarded as waste. Thus, and at the present time, the interferometer uses merely 12.8% of its full-aperture capability. This reduces the number of photons entering the interferometer and results in approximately a fourth magnitude brightness limit. There are about 6,000 stellar objects available to

*Address all correspondence to: James H. Clark, III, E-mail: jimclark189@gmail.com

Fig. 1 Aerial view of the Navy Precision Optical Interferometer (NPOI) site, Flagstaff, Arizona (Photo courtesy of Michael Collier).

the interferometer of magnitude 4 or brighter. The unexploited portion of light reflected from the primary mirror is simply absorbed or reflected away by structures and objects surrounding the tip–tilt mirror. Figure 3 depicts a typical siderostat station showing the stellar light path reflected from the 38-cm siderostat (35-cm clear aperture) to the active tip/tilt mirror with and without the beam compressor.

The transport optics,[3] beginning inside the ported cylinder just beneath the tip/tilt mirror in Fig. 3, is housed in an evacuated piping system, along a Y-array configuration (see Fig. 1), the arms of which range out to 240 m in length. This evacuated transport system provides transfer of the stellar wave fronts (optical beams), up to nearly 800 m in horizontal length that are 1 to 2 m above ground level, to the beam combiner without generating additional thermally induced wavefront distortions such as those that naturally occur from the earth's thick atmosphere. The combination of primary aperture, 38 cm, and fast active tip/tilt mirror suffices to eliminate the requirement of adaptive optics. Larger-aperture telescopes, e.g., 1.4-m portable lightweight and stationary 1.8 m Keck outriggers, will employ adaptive optics to correct for higher order aberrations and utilize the current evacuated transport system.

The prospect of obtaining an eightfold increase in stellar observables by simply assembling and installing previously acquired compressor mounts and optics is quite appealing. However, as discussed in a previous paper,[4] the as-built mount exhibits excessive vibration characteristics that require addressing prior to bench testing the optics and on-site NPOI alignments. Furthermore, the as-built primary mirror for the compressor was discovered to be asymmetric about its geometric center. It is 1.3-cm thicker at the top than at the bottom, generating speculation that it may sag excessively and nonuniformly once down-tilted 20 deg to the operational orientation. Therefore, the present work was initiated to characterize deviations of the reflective surface on the primary mirror with respect to tilt angle and, if necessary, to perform a first-order analysis to determine whether a simple conceptual mechanical counterweight-type fix is feasible.

1.2 *Historical Background*

Off-axis beam compressors were envisioned and planned for in the early years of the NPOI, circa 1990. Placeholders, in the form of concrete piers, were even installed during the site construction phases, which began in the year 1993. These piers are located between the siderostat and active tip/tilt mirror. The off-axis beam compressor optics and mounts were procured, circa 2004. The mounts were determined to be inadequate in a natural vibrational frequency, and a subsequent analysis was performed to determine if simple mechanical modification would adequately stiffen the mount and increase its natural frequency.[5] Further effort, including the focus of this article, is underway to determine the magnitude of the deflection of the primary mirror when tilted down at 20 deg relative to the horizontal. The mirror, during fabrication, was measured and verified to be within specification, while oriented in the stand-up (zero-tilt angle) position. The maximum peak-to-valley resultant wavefront error of the two-mirror compressor was specified to be less than or equal to 63 nm across the clear aperture.[6] It is not known

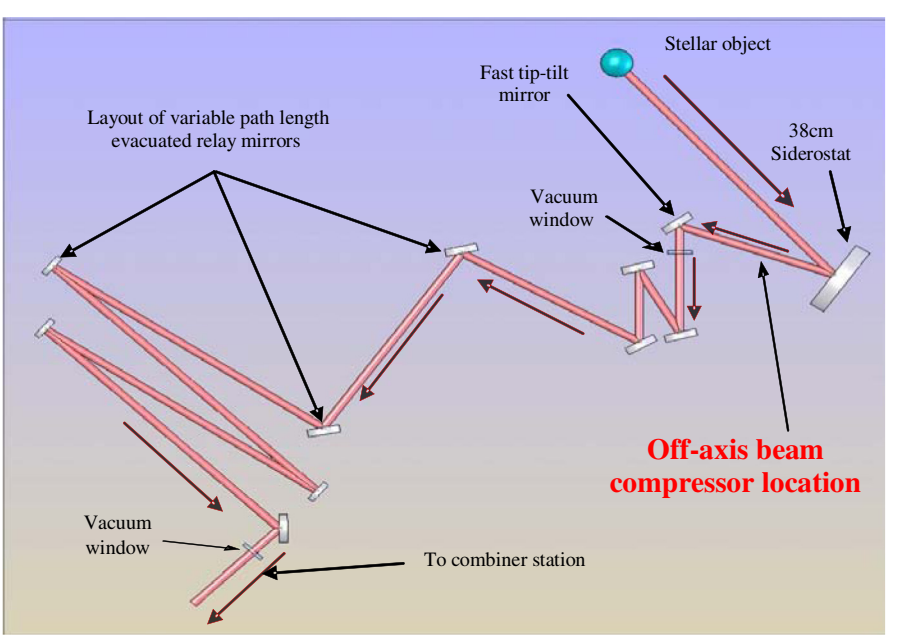

Fig. 2 Schematic of typical optical station light path showing location of the off-axis beam compressor.

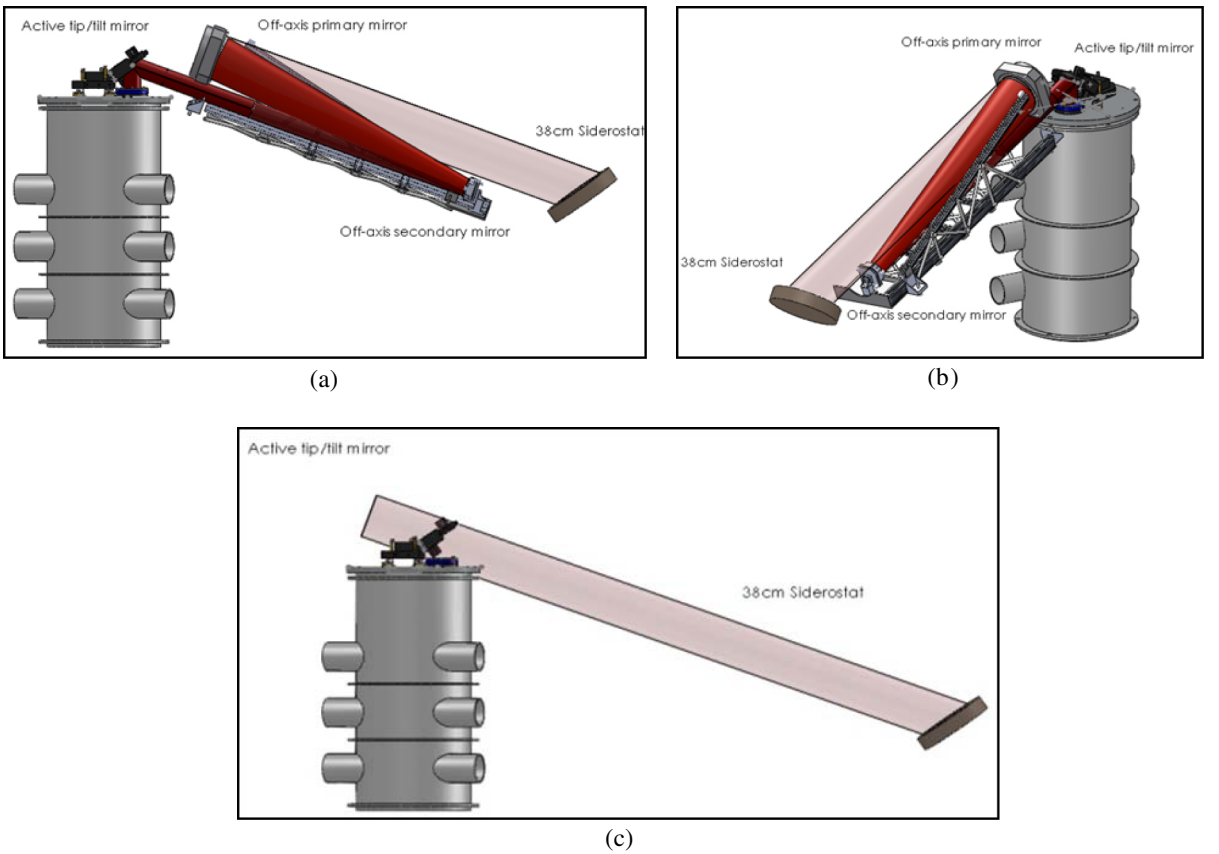

Fig. 3 Typical siderostat station. (a) Location of the off-axis beam compressor between siderostat and tip/tilt mirror. (b) Isometric view of typical siderostat station with beam compressor. (c) Siderostat station sans beam compressor, also the present configuration at the NPOI.

what level of engineering analysis occurred regarding the body geometry and constraints of the primary mirror relating tilt angle and surface deformation; no documentation could be found. Figure 4(a) shows a test fit of the as-built mount, circa 2005, and indicates the size/scale of the compressor. Figure 4(b) shows the mount fitted to the concrete pier and tilted downward at the 20-deg service angle. The siderostat is located just outside the latter figure and to the right.

Laboratory-based optical tests were conducted at our local Navy facility, circa 2006. The mount exhibited unacceptable resonant vibrational characteristics so severe, from an interferometric viewpoint, that alignments could not be properly accomplished and experimental measurements of the performance at the 20-deg down-tilt were not obtainable.

1.3 *Description of As-Built Beam Compressor Assembly*

The as-built beam compressor assembly consists of primary and secondary Zerodur® mirrors held in place by an aluminum alloy mount, as illustrated in Fig. 5. There are three equally spaced front pads, three corresponding and opposing rear pads for constraining each mirror along the optical axis, and four adjustable radial screws (diametrically opposed) to

Fig. 4 Simple mechanical test fit of beam compressor mount in astrometric station. (a) Compressor being lowered into astrometric station. (b) Compressor fitted to concrete pier between fast tip–tilt mirror (upper left) and siderostat (outside view to right) at the 20-deg down-tilt operational angle.

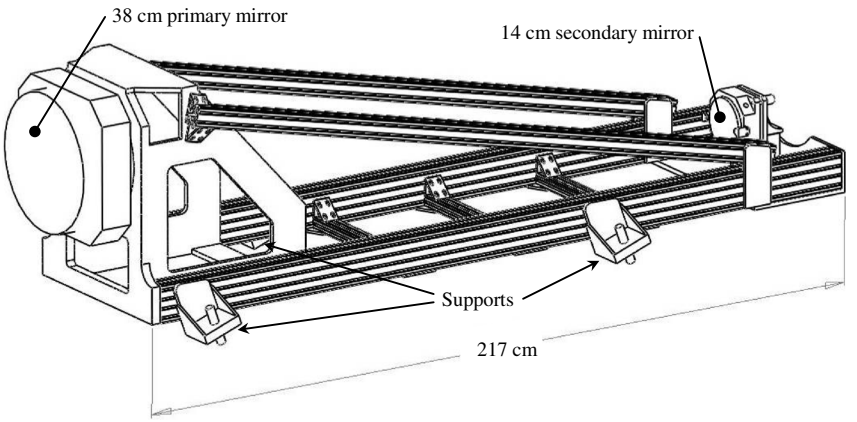

Fig. 5 Original design of the off-axis beam compressor mounts. All components, except the mirrors, are made of aluminum.

provide support at the circumference of each mirror. The primary mirror is an off-axis segment of a concave parabolic "parent" mirror of nominal focal length $F_p = 3111$ mm. The off-axis segment is 38 cm in physical diameter with a clear aperture of 35 cm and centered at 41 cm from the axis of the parent mirror.[6] The back surface is flat and perpendicular to the optical axis. The as-built front-to-back thickness of the primary mirror varies: the upper portion is 10.2-cm thick and the lower portion is 8.9-cm thick.

The secondary mirror is an off-axis segment of a convex parabolic "parent" mirror of nominal focal length $F_s = -1111$ mm. The off-axis segment is 14 cm in physical diameter with a clear aperture of 12.5 cm and centered at 14.6 cm from the axis of its parent mirror. It is considered that, regardless of whether the aluminum mount is worth salvaging, the mirrors should be analyzed to determine their surface deflection characteristics over a range of tilt angles.

1.4 *Objective*

Our objective in this work is to determine what changes occur in the front reflective surface of the off-axis primary mirror due to changes in tilt angle and whether these changes can be counteracted with a simple mechanism. Specifically, we investigate, as a first pass to determine feasibility for correcting the mirror, the response of the front reflective surface of the primary mirror when tilted down 20 deg. Matched sets of primary/secondary mirrors were ground, polished, and figured at the fabricator's shop while lying on their back surfaces, and the pair was stood up on their edges and optically measured to verify that they met the 63-nm peak-to-valley total error specification for the optical view facing the horizontal orientation. We have no records that the pair of mirrors was ever optically measured in the 20-deg down-tilt angle, and hence, no experimental data to compare. Due to the geometry of the primary mirror body, thicker at the top than the bottom, nonsymmetric deformation sag due to tilt angle is suspected. Fortunately, the beam compressor assembly is designed to be statically mounted to its pier, as a nontracking optical device, and it is therefore conceivable that simple antisag mechanisms could be fashioned that return the front surface figure to within the tolerance specification.

We first analyze the mirror surface deflections under earth-gravity conditions representing various down facing tilt angles using the finite element method (FEM). Then, at the operational tilt angle of 20 deg, we apply outward forces on the back surface of the mirror to counteract the sagging effect and discuss the results. Furthermore, the process followed and the results obtained can be useful as guides for engineers and scientists involved in the design of similar optomechanical structures.

2 Finite Element Analysis

2.1 *Overview of FEM*

FEM is a numerical technique that provides approximate solutions to a wide variety of engineering problems. The region of interest is divided into an assemblage of smaller subregions, or elements, having simple geometries and interconnected by nodes on the element boundaries. Continuous piecewise smooth functions over the element region are used to approximate the unknown functions within the element. These functions, known as interpolation functions, are typically selected as polynomials, because they are easy to integrate and differentiate. The basis of the method is that the global response of the structure is the summed response of the responses of the individual elements. By using an integral formulation, usually derived from an energy approach, a system of algebraic equations in the unknown nodal quantities is generated. It can be shown that the method converges to the exact solution as the size of the elements is made smaller. The method has gained substantial popularity in recent years, and a variety of commercially available programs is presently available. The mathematical foundations of the method, as well as its application to structural problems such as the mirror analysis described below, are well established, and the details can be found in the literature.[7,8] For the present work, we have chosen COSMOS/M,[9] a complete, modular, self-contained finite element system developed by Structural Research and Analysis Corporation for personal computers and workstations.

2.2 *Finite Element Model*

In order to determine the front surface deflections of the primary mirror, a finite element model was built and run using

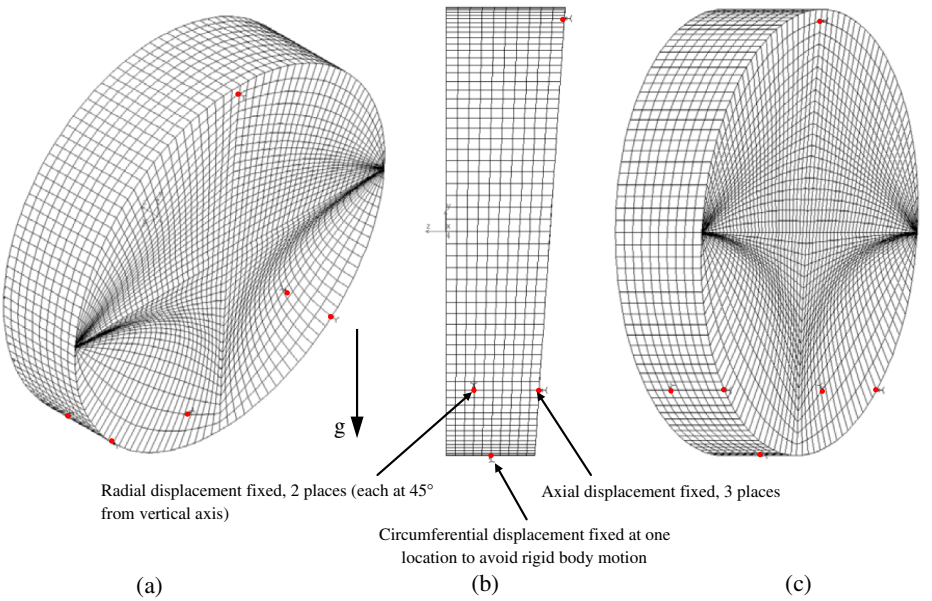

Fig. 6 Finite element mesh and boundary conditions used in the model of the primary mirror. (a) Isometric view. (b) Side view. (c) Side-angle view. Displacement boundary conditions are shown as dots with an arrow pointing in the displacement direction.

COSMOS/M.[9] The mesh and boundary conditions used to model the original configuration are shown in Fig. 6.

This figure also labels the different components of the mirror. The nodal displacements in appropriate directions, as shown in Fig. 6, were set to zero at the nodes corresponding to the supports in the actual mirror. The model consisted of 24,000 20-noded solid elements. The number of nodes in the model was 103,861. The properties used for the Zerodur® glass material are shown in Table 1.

3 Analysis of Primary Mirror

The baseline mirror shown in Fig. 6 was first analyzed in the standing-up position (zero-tilt angle) with the optical axis of the mirror horizontal and under −1 g upward body-force conditions. The absolute value of the y-component of the gravitational body force is equal to 1 g, and that of the z-component is equal to 0 g. The resulting nodal displacements for the optical z-axis are shown in Fig. 7(a), and the surface contour is what might be expected if the mirror were fabricated perfectly on earth, under 1 g conditions, and then taken to outer space. The $+z$ displacements seen in the upper regions indicate that the thickness has thinned, as would be expected if this mirror were imagined to be allowed to relax and stretch in the absence of gravity. Shown in Fig. 7(b) is the finite element analysis result after applying +1 g (downward) body forces directly to the baseline mirror. In this case, the absolute value of the y-component of the gravitational body force is again equal to 1 g, and that of the z-component is equal to 0 g, but the direction of g has flipped 180 deg. The resulting surface contour is analogous to what would be expected if the mirror were perfect in 0-g conditions, then brought to earth, stood up, and supported as depicted in Fig. 6.

Table 1 Mirror properties used in the analysis.

Property	Glass (Zerodur)[9]
Modulus of elasticity, E (GPa)	90.3
Poisson's ratio, ν	0.243
Density, ρ (kg/m^3)	2530

Proper simulation of the sag of the actual as-built mirror in the standing position requires us to superpose the x-, y-, and z-coordinates of the nodal displacement results shown in Figs. 7(a) and 7(b). This is performed as the sum of the associated nodal coordinate displacements from both cases, i.e., $(+1\text{ g}) + (-1\text{ g})$. The analysis results of this superposition, shown in Fig. 8(a), aptly indicate zero surface displacement. It is what would be expected if the optician fabricated a perfect mirror, as measured in the standing position with supports and boundary constraints shown in Figs. 6(b) and 6(c), on the surface of the earth.

In the determination of surface-sag versus tilt angle, the −1 g nodal displacement results were superposed with those obtained from analyses cases using discrete-angled orientations of the gravity vector. The mirror was not tilted in the finite element model; rather, the angle of the gravity vector was changed with respect to the mirror body. This had the additional benefit of retaining common points of reference such as coordinate and optical axes. The x-component in this entire study remains zero, since there is no roll anticipated in mounting and positioning the beam compressor at the NPOI. Six analyses cases were run on the baseline model from 0 to 25 deg in 5-deg increments. The 0-deg case corresponds to the validation measurement orientation of the physical mirror during manufacturing and represents our zero-sag starting point. The 25-deg case, 20% beyond the operational 20-deg down-tilt angle, was arbitrarily chosen as a convenient maximum down-tilt orientation, while increments of 5 deg were chosen for our first-pass analysis and could readily be increased if sensitivity in the results revealed

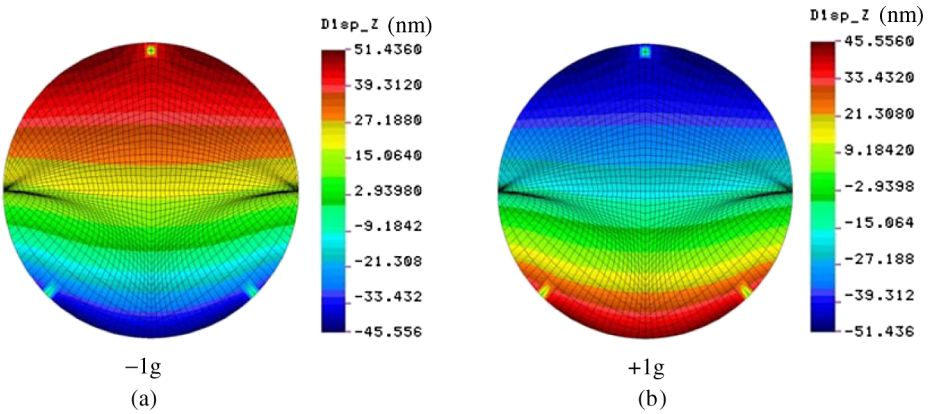

Fig. 7 Displacement contour plots. (a) Gravity load −1 g (upward). (b) Gravity load +1 g (downward). The +*z*-axis is facing directly into the page of the paper (corresponding to axis orientation shown in Fig. 6).

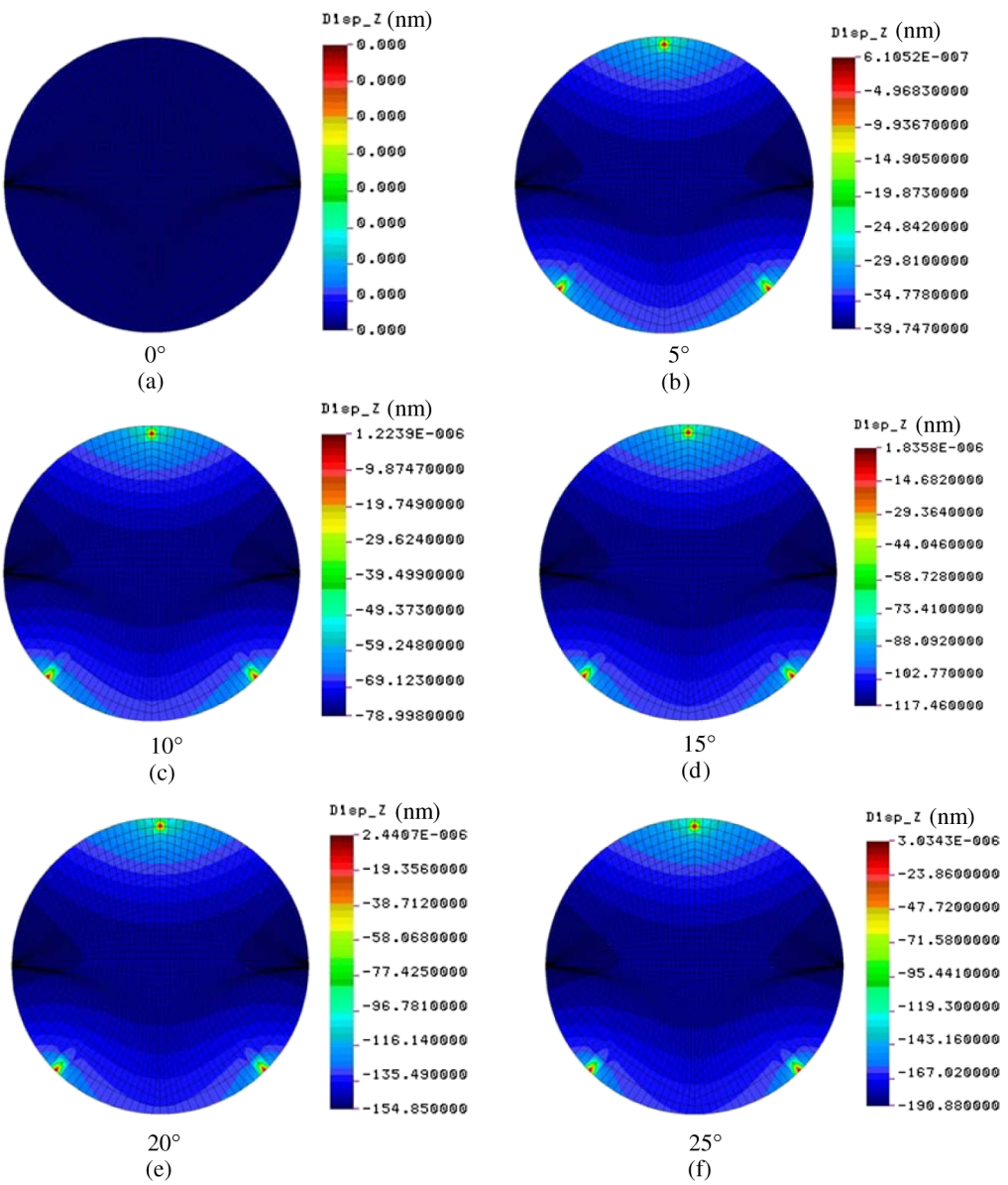

Fig. 8 Displacement versus down-tilt angle as viewed from the optical *z*-axis. (a) 0-deg tilt. (b) 5-deg tilt. (c) 10-deg tilt. (d) 15-deg tilt. (e) 20-deg tilt. (f) 25-deg tilt. Displacements are in nm and angles in degrees.

the necessity. In the 5-deg case, for example, the magnitude of the downward y-component of gravity was 0.9962 g, that along the negative optical z-axis was 0.0872 g, and that corresponding to the lateral x-axis remained 0. These results were subsequently superimposed with the results for the -1 g case. The z-axis was parallel to the optical axis and perpendicular to the mirror's back surface for each case. The z-axis contour plots are shown in Figs. 8(a) through 8(f); each set of results shown has been superposed with the -1-g baseline nodal displacements. These displacements are viewed parallel to the optical axis.

Figure 8(e) corresponds to the NPOI operational down-tilt angle of 20 deg and shows that the mirror sag is 155-nm peak-to-valley in the optical axis. This magnitude of sag represents a factor of 2.5 times the allowable wavefront distortion, $\lambda/10$, of the combined primary and secondary mirrors. It is also 134 nm beyond our allowable tilt-induced sag of 21 nm, as explained below.

The specification for the resultant wavefront deformation of the combined primary and secondary mirrors is $\lambda/10$ peak-to-valley across the clear aperture, where $\lambda = 633$ nm. Therefore, the maximum resultant deformation relative to a mathematically perfect surface is 63 nm. Five pairs of these mirrors were fabricated as matched sets with maximum resultant wavefront errors equal to or less than $\lambda/15 =$ 42 nm, well within the specification. Figure 9 shows a contour plot of one such set of matched mirrors and indicates peak-to-valley deformation equal to 0.0534 $\lambda = 34$ nm and an RMS value equal to 0.0642 $\lambda = 41$ nm over 100% of the aperture. Other pairs of mirrors have peak-to-valley deformations near 42 nm. Therefore, for the purposes of this analysis, we allow a further tilt-induced deformation

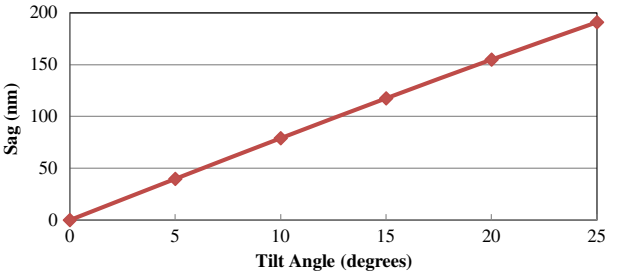

Fig. 10 Peak-to-valley deformation versus down-tilt angle of as-built primary mirror.

of 21-nm peak-to-valley. This value corresponds to the maximum allowable induced sag under any tilt angle. The mirror pairs were initially aligned, optically measured, and verified by the fabricator while standing up on their edges with the optical axis parallel to the horizon. This corresponds to our 0-deg tilt case described in the previous section. Our operational orientation, however, is at the 20-deg down-tilt angle, such that the primary mirror faces downward. Furthermore, we assume the secondary mirror, having a relatively small surface area, remains constant when faced up at 20 deg, leaving the 21 nm of allowable surface sag entirely for the primary mirror. Figure 10 plots the peak-to-valley deflection of the primary mirror versus downward orientation angle.

Maximum surface deformation versus tilt angle is nearly linear in relationship, even though the mirror segment is asymmetrical (thicker at the top than bottom). Because we are investigating maximum peak-to-valley results only, further analysis, such as ray tracing, is required to determine the subtle aberration effects from any slight asymmetrical

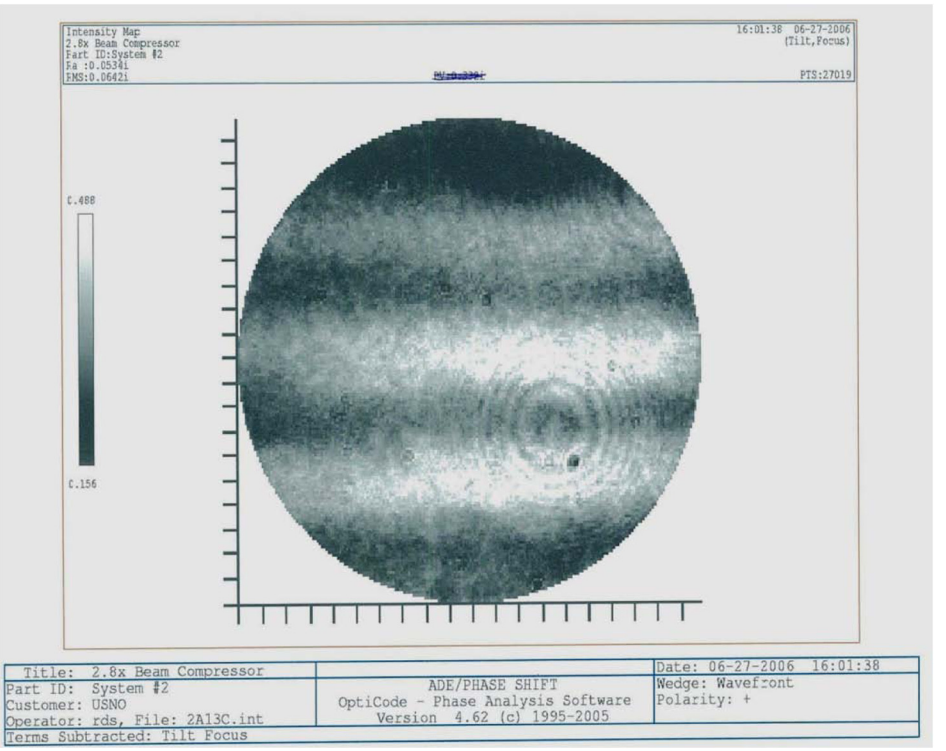

Fig. 9 Wavefront measurement contour for a matched primary/secondary set of mirrors. Peak-to-valley deformation over 100% of surface equals 34 nm.

sag behavior. The 21-nm distortion deformation limit occurs at 2.8-deg tilt, whereas 155-nm sag occurs at our operational 20-deg tilt. This is 134 nm outside our allowable sag and represents a peak-to-valley ratio of only $\lambda/4$. The question becomes whether there is a simple passive fix that counteracts the sag sufficiently and returns the surface deviations to less than a peak-to-valley displacement of 21 nm. This is discussed in the next section.

4 Design Modifications to Reduce Angle-Induced Sag

Results from the previous section indicate that 155-nm peak-to-valley surface aberrations occur when the primary mirror tilts down to the operational angle of 20 deg. We allow no more than 21-nm tilt-induced sag on the as-built mirror and are therefore 134 nm beyond this tolerance. We now explore the feasibility of a simple counteracting device to reduce the magnitude of mirror sag. The concept of a simple mechanical device attached to the back surface of the mirror that pulls outward to reduce tilt-induced sag on the front surface is the preferred solution path for a first-order correction. The device is conceived of as levered mechanisms with flexure pivots, one end attached to Invar® pucks and the other to the mirror cell. The pucks are adhered to the back surface of the mirror. Counter weights would be attached to the levers in such a way that a pull force is applied to the pucks. The pucks serve as load distributors and reduce stress concentrations in the Zerodur® material. Alternate concepts include simple adjustable extension springs attached to the pucks. The details of the mechanism are left for future work. As a research model for this concept, finite element analyses were run using four forces applied to the back surface of the mirror and in the $+z$ direction. The magnitude of each force was 17.8 N with approximate locations, as shown in Fig. 11.

The constraints and gravity loading applied to the mirror remain the same as in the 20-deg down-facing analysis case. The maximum peak-to-valley displacement after applying this corrective force system reduces to 32 nm. Although 14 nm beyond the allowable 21-nm sag and 33% outside the tolerance, the improvement is very substantial. The results, with numerical values shown in the legend of Fig. 12, also indicate a more uniform sag distribution on the reflective surface when compared with the results shown in Fig. 8(e), the noncounteracted 20-deg down-tilt angle. The resultant

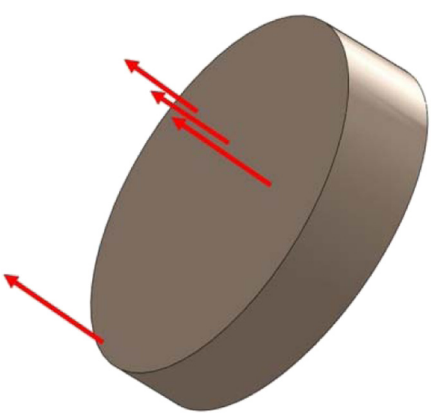

Fig. 11 Forces applied to the back surface of mirror as first-order sag correction.

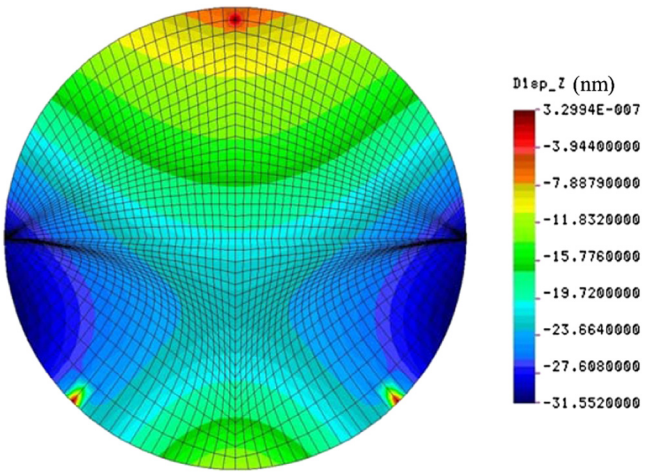

Fig. 12 Displacement contour plot of 20-deg down-tilt with four 17.8-N forces applied to the backside of mirror.

wavefront specification for the combined primary and secondary mirrors is $\lambda/10$ (63 nm) peak-to-valley. The as-built maximum peak-to-valley displacement, at 20-deg down-tilt angle, reduces the wavefront quality to only $\lambda/4$ (155 nm), but with counter-force correction, it improves to $\lambda/20$ (32 nm). Applying the as-built assured resultant of $\lambda/15$ (42 nm) to the tilt-induced but with counter-forced result, $\lambda/20$ (32 nm), implies a combined primary and secondary results of $\lambda/8.6$. It should be noted that the location, magnitude, quantity, and other such details of this counteracting force system are not optimized, as the intent of this analysis is to show feasibility only. Furthermore, ray trace analysis and experimental data will further determine the suitability of this as-built mirror and any corrective measures applied to it. For the purposes of this preliminary first-order analysis, however, it appears that a simple passive counter-acting force system induces enough counter sag at 20-deg down-tilt to salvage this mirror for NPOI applications.

5 Conclusions and Recommendations

An analysis of sag versus tilt angle of an asymmetric off-axis parabolic as-built primary beam compressor mirror, for use at the NPOI, was performed using the finite element analysis technique. The maximum aberrated wavefront of the combined as-built primary and secondary mirror pairs is specified to be not greater than $\lambda/10$, where $\lambda = 633$ nm, the wavelength of a helium neon laser used to measure the surface contour, and so corresponds to a combined allowable wavefront deviation of 63 nm. We determined the maximum allowable tilt-induced peak-to-valley deformation of the primary mirror surface to be 21 nm and found this to occur at 2.8-deg down-tilt angle. At the NPOI operational down-tilt angle of 20 deg, however, the peak-to-valley displacements increase to 155 nm, 134 nm beyond our allowable. A first step to determine feasibility that a design modification concept to reduce tilt-induced sag, in the form of simple pull forces on the rear surface of the mirror, was investigated and found to be a feasible solution path. Four outwardly applied 17.8-N forces on the rear surface of the mirror reduce the sag from 155 nm to 32 nm at the 20-deg down-tilt. This results in combined wavefront aberration of $\lambda/8.6$ for the output of the as-built beam compressor and is considered

a viable and economic solution path to an expensive set of optical components. The deviated wavefront of $\lambda/10$ was not quite achieved, and therefore additional effort remains to reduce tilt-induced sag on this mirror. An adaptive optics solution was not considered necessary due to the present combination of relatively small aperture and fast tip/tilt correction for the NPOI site. Future work consists of designing and analyzing the mirror in more detail to optimize the location, magnitude, and quantity of the passive counter-acting force system and its influence on the mirror surface. In addition, we propose to perform ray-trace analysis to determine more precisely the effects of surface irregularities and thermal influence on alignments and management of the optical surfaces in an exposed environment.

Acknowledgments

This work was funded in part by the Naval Research Laboratory (NRL) as part of a collaborative effort between NRL and Northern Arizona University toward improving the engineering and scientific performance of the Navy Precision Optical Interferometer and advancing the associated technology.

References

1. J. T. Armstrong et al., "The Navy Prototype Optical Interferometer," *Astrophys. J.* **496**(1), 550–571 (1998).
2. F. E. Penado and J. H. Clark III, "Optimizing the frequency response of a steering mirror mount for interferometry applications," *Proc. SPIE* **7424**, 742403 (2009).
3. J. H. Clark, III et al., "Mount-induced deflections in 8-inch flat mirrors at the Navy Prototype Optical Interferometer," *Proc. SPIE* **7013**, 70133K (2008).
4. F. E. Penado, J. H. Clark, III, and F. Cornelius, "Stiffening an off-axis beam compressor mount for improved performance," *Proc. SPIE* **7793**, 77930G (2010).
5. T. Woods, E. Hardman, and B. Cook, "NPOI—big beam compressor stabilization," Final Report for Senior Capstone Design Project, Mechanical Engineering Department, Northern Arizona University (2010).
6. D. Hutter, Specifications (preliminary): off-axis beam compressor mounts [Internal NPOI documentation] (2010).
7. O. C. Zienkiewicz, R. L. Taylor, and J. Z. Zhu, *The Finite Element Method: Its Basis and Fundamentals*, 7th ed. Elsevier, New York (2013).
8. K. H. Huebner et al., *The Finite Element Method for Engineers*, 4th ed., John Wiley & Sons, New York (2001).
9. Structural Research and Analysis Corporation, *COSMOS/M User's Guide, Version 2.95*, Structural Research and Analysis Corporation, Los Angeles (2007).

James H. Clark, III is the chief mechanical engineer at the Navy Precision Optical Interferometer in Flagstaff, Arizona. Previously, he worked at Optelecom Inc. on fiber optic payout systems for unmanned guided vehicles. His research interests include solid mechanics and optomechanical systems. He works closely with Northern Arizona University in applications related to the NPOI, and currently teaches classes as a part-time instructor in mechanical engineering and sponsors senior engineering capstone projects

F. Ernesto Penado is professor and chair of the Department of Mechanical Engineering at Northern Arizona University. His areas of interest include composite materials, solid mechanics, and optomechanical systems. He received his PhD in engineering mechanics from the University of Utah in 1987 and worked in the aerospace industry prior to joining academia in 1994. The results of his research work have been published in numerous scholarly articles and presented at various technical meetings